Selective esterase–ester pair for targeting small molecules with cellular specificity

Lin Tian[1], Yunlei Yang, Laura M. Wysocki, Alma C. Arnold, Amy Hu, Balaji Ravichandran, Scott M. Sternson, Loren L. Looger, and Luke D. Lavis[2]

Janelia Farm Research Campus, Howard Hughes Medical Institute, 19700 Helix Drive, Ashburn, VA 20147

Edited by Carolyn R. Bertozzi, University of California, Berkeley, CA, and approved January 18, 2012 (received for review July 22, 2011)

Small molecules are important tools to measure and modulate intracellular signaling pathways. A longstanding limitation for using chemical compounds in complex tissues has been the inability to target bioactive small molecules to a specific cell class. Here, we describe a generalizable esterase–ester pair capable of targeted delivery of small molecules to living cells and tissue with cellular specificity. We used fluorogenic molecules to rapidly identify a small ester masking motif that is stable to endogenous esterases, but is efficiently removed by an exogenous esterase. This strategy allows facile targeting of dyes and drugs in complex biological environments to label specific cell types, illuminate gap junction connectivity, and pharmacologically perturb distinct subsets of cells. We expect this approach to have general utility for the specific delivery of many small molecules to defined cellular populations.

cellular imaging | microscopy | enzyme substrates | fluorophores | pharmacological agents

Chemical probes are essential tools in biology for measuring and manipulating cellular properties. Optimization of the structural and electronic features of small molecules allows the fine-tuning of molecular recognition specificity for a particular cellular target. Even with high molecular specificity, however, the application of small molecules in complex biological environments is frequently limited by poor cellular specificity. The inability to target small molecules, such as imaging or pharmacological agents, to defined cellular populations can confound the evaluation and control of discrete subsets of cells within a multicellular environment. A general and efficient strategy for cell-specific targeting, combining the molecular specificity of small molecules with the cellular specificity of genetics, would allow intracellular pathways in defined cell types to be selectively probed in complex tissues.

An attractive approach for general cell-specific delivery of small molecules employs selective enzyme–substrate pairs. In this strategy, compounds are masked by attachment of a standard, disposable blocking group that is stable to native cellular enzymes, but labile to a specific exogenous enzyme. Expression of such a protein in a genetically defined cell population permits unmasking of the small molecule with cellular specificity. To be useful across experimental paradigms, such a system should utilize an enzyme that unmasks molecules with high efficiency, expresses in different cell types, and exhibits low cellular toxicity. The cognate masking group must be modular, synthetically efficient, and allow molecules to diffuse passively across the cellular membrane, while also exhibiting favorable solubility and stability in aqueous solution.

To date only a few enzyme–substrate pairs have been used as targeted delivery systems for small molecules, and none meet all the criteria outlined above. Strategies employing enzymes encoded by common reporter genes (1) have found some success in targeting small molecules (2–4), but the selectivity and efficiency of these systems is eroded by several factors. For example, alkaline phosphatase substrates are most effective extracellularly, and targeting using this enzyme has been limited to membrane probes (4). β-Galactosidase substrates display only modest membrane permeability (2), and are further restricted by competing native enzyme activity (5). β-Lactamase substrates are large, synthetically complex, and exhibit poor chemical stability and tissue penetration (1, 3). Catalytic antibodies have been designed for small molecule targeting, but these systems suffer from poor cellular expression and slow unmasking kinetics (6). Gene therapy research has identified intriguing enzyme–substrate pairs and used these systems to target particular cytotoxic agents to tumor cells (7, 8). Although useful for cell ablation studies (9), these systems have not been generalizable for molecular targeting. Overall, the existing enzyme–substrate pairs are incompatible or inadequate for the majority of applications, and thus enzyme-mediated small molecule targeting is rarely used in biology.

Given these limitations, we set out to develop a general and efficient enzyme–substrate system to deliver small molecules with cellular specificity. We surmised a selective esterase–ester pair could be an attractive strategy for cell-specific unmasking of small molecules. Esters have many advantages as masking moieties: they are simple to synthesize, can mask a variety of functional groups, and render molecules cell permeable. Indeed, chemical derivatization with esters reactive to endogenous esterases is an established and effective strategy to deliver compounds to cells in many contexts (10, 11). Moreover, exogenous esterases can be expressed heterologously; carboxylesterases from different species have been used to enrich an anticancer agent (7) or a calcium indicator (12) in specific cells and subcellular locales.

Nevertheless, esters and esterases present challenges for cell-specific small molecule delivery. Many esters show appreciable rates of enzyme-independent hydrolysis, and cellular esterases show broad substrate reactivity (13, 14). Both of these pathways can degrade cell specificity of an ester-masked small molecule by leading to accumulation of the unmasked compound in all cells. The aforementioned expression of exogenous esterases can improve small molecule targeting (7, 12), but current systems use ester masking groups that are also reactive to endogenous esterases, leading to incomplete cellular selectivity. To overcome these stability and selectivity problems, we explored synthetic branched esters, as substitutions on the α-carbon can increase chemical stability (15) and cellular esterases can exhibit surprising selectivity toward complex esters (11, 16). To quickly identify a selective esterase–ester pair, we prepared a series of unique, chemically stable fluorogenic esterase substrates bearing different ester functionalities. We leveraged the ease of fluorescence techniques to rapidly find a small, chemically stable ester that is resistant to hydrolysis by native esterases, and then screened

Author contributions: L.T., S.M.S., L.L.L., and L.D.L. designed research; L.T., Y.Y., L.M.W., A.C.A., A.H., B.R., and L.D.L. performed research; L.T., Y.Y., L.M.W., S.M.S., and L.D.L. analyzed data; and L.T., S.M.S., L.L.L., and L.D.L. wrote the paper.

The authors declare no conflict of interest.

This article is a PNAS Direct Submission.

Freely available online through the PNAS open access option.

[1]Present address: Department of Biochemistry and Molecular Medicine, University of California, Davis, Sacramento, CA 95817.

[2]To whom correspondence should be addressed. E-mail: lavisl@janelia.hhmi.org.

This article contains supporting information online at www.pnas.org/lookup/suppl/doi:10.1073/pnas.1111943109/-/DCSupplemental.

exogenous enzymes to determine an esterase capable of catalyzing the hydrolysis of this ester bond. We then characterized the efficacy of this unique enzyme–substrate pair to target different imaging and pharmacological agents in cell culture and brain tissue with cellular specificity.

Results and Discussion

Identification of a Selective Esterase–Ester Pair. To find an ester motif resistant to cleavage by endogenous esterases, we synthesized a series of fluorogenic esterase substrates based on the chemically stable fluorescein di(acetoxymethyl ether) (fluorescein-AM_2, **1**, Fig. 1*A*) (17). Compounds **2**–**6** were prepared by the efficient reaction of iodomethyl esters with fluorescein in the presence of Ag_2O (Fig. S1*A*). We limited this series to contain small, commercially available, achiral esters with different α-carbon substitution patterns encompassing a range of steric and stereoelectronic properties. Compounds **1**–**6** show low background fluorescence in the masked form, and hydrolysis of the ester bonds ultimately releases the bright green fluorophore, fluorescein (17). In addition to high contrast, chemical stability is important for accurate determination of cellular esterase activity. Each of these masked fluorophores is cleaved remarkably slowly by the esterases present in tissue culture media ($t_{1/2} \geq 12$ h) and exhibits high stability in simple aqueous solutions ($t_{1/2} \gg 4$ d; Fig. S2). These substrates are therefore ideal for accurate, rapid assessment of esterase activity inside living cells, being simple to synthesize and resistant to spontaneous hydrolysis in cell culture conditions.

The substrate specificity of native cellular esterases was investigated by incubating different cell lines and tissue with molecules **1**–**6** followed by wide-field or two-photon fluorescence microscopy (Fig. 2). Images are given in Fig. 2 *A*–*F*, and average cellular fluorescence for each tissue sample and substrate is quantified in Fig. 2*G*. These experiments revealed interesting substrate specificity of endogenous cellular esterases across cell types, indicating divergent activity toward synthetic substrates. Simple ester substrates **1** and **2** were unmasked in all cell lines tested, consistent with the expected high activity of native esterases for straight-chain esters (Fig. 2 *A* and *B*). Cyclobutyl ester **3** showed partial selectivity; it was an excellent substrate for esterases expressed in most mammalian cells, but was not cleaved in *Drosophila* S2 cells (Fig. 2*C*). The methacrylate substrate **4** also showed differential reactivity, as it was unmasked in cells from most rodents, but not significantly in cells from human or fly (Fig. 2*D*). The pivaloyl substrate **5** remained masked in cultured cells including rat dissociated neurons, but was hydrolyzed in mouse brain tissue (Fig. 2*E*). Only the fluorescein di(1-methylcyclopropanecarboxymethyl ether) substrate (**6**, fluorescein-CM_2) remained masked in all cultured cell lines and brain slice (Fig. 2*F*), showing this stable ester is resistant to hydrolysis by endogenous esterases in numerous cell types from different species. α-Cyclopropyl esters are known to exhibit extremely high chemical stability due to a combination of steric and stereoelectronic effects (15).

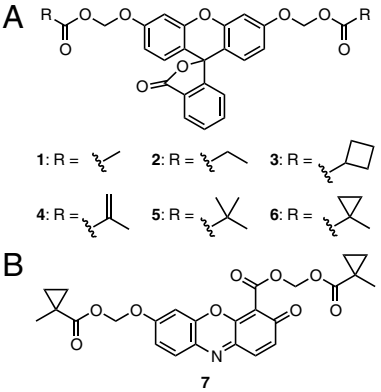

Fig. 1. (*A*) Chemical structures of masked fluorophores **1**–**6**. (*B*) Chemical structure of masked fluorophore **7**.

We then sought an exogenous esterase capable of cleaving the stable ester bond in fluorescein-CM_2. We recognized that other chemically stable α-cyclopropyl esters, such as the pyrethroid insecticides, can be cleaved readily by some esterases (18). Thus, we incubated substrate **6** with a panel of commercially available esterases and lipases from a variety of organisms (Fig. S3*A*). Only porcine liver esterase (PLE) (19) efficiently cleaved cyclopropyl substrate **6**. We determined the catalytic constants of PLE unmasking of fluorescein-CM_2 (**6**) and compared them to the unmasking of fluorescein-AM_2 (**1**) as shown in Fig. S3 *B* and *C*. Masked fluorophore **1** was cleaved by PLE with apparent catalytic constants $k_{cat}/K_M = 5.8 \pm 0.9 \times 10^5$ M^{-1} s^{-1} (mean ± SE) and $K_M = 2.7 \pm 0.4$ μM, in agreement with previously published values (17). The CM derivative **6** was cleaved more slowly, exhibiting apparent catalytic constants of $k_{cat}/K_M = 5.1 \pm 0.5 \times 10^4$ M^{-1} s^{-1} and $K_M = 0.50 \pm 0.05$ μM. Although fluorescein-CM_2 is resistant to hydrolysis by water, biological nucleophiles, and many endogenous enzymes, the cyclopropyl substitution causes only a modest and acceptable reduction in the catalytic efficiency of PLE against this substrate.

Esterase-Mediated Unmasking in Cells. Having established PLE and the α-cyclopropyl ester in compound **6** as a potential selective esterase–ester pair, we next evaluated the utility of this PLE–CM system in living cells. Based on previous examples of heterologous esterase expression (7, 12), we utilized the full-length coding sequence for the enzyme, preserving the N-terminal lipophilic signal sequence and the C-terminal His-Ala-Glu-Leu retention motif (Fig. S3*D*). Such amino acid sequences direct esterases to the endoplasmic reticulum (ER) (7, 20). Expression of PLE in HeLa cells yields a functional enzyme that is able to rapidly cleave substrate **6** (Fig. S4*A*, Movie S1). Mutation of the catalytic triad of PLE (S222A/E354A/H467A) prevented the unmasking of fluorescein, showing that active PLE is necessary for ester hydrolysis (Fig. S4*B*). In addition, deletion of the N-terminal lipophilic signal sequence yielded no fluorescein unmasking in cells (Fig. S4*C*), suggesting that trafficking to the ER is essential for enzymatic activity. Based on this result we investigated the subcellular localization of PLE. Insertion of the cyan fluorescent protein mCerulean3 sequence (21) after the N-terminal signal sequence confirmed the protein is localized in the ER (Fig. S4*D*). The unmasked fluorescein is not restricted to the ER, but found throughout the cell, including the nuclear compartment, as shown in Fig. S4*E*, due to the small molecule permeability of the ER membrane (22, 23). We estimated the amount of enzyme and unmasked fluorophore in a cell by confocal microscopy (24). Approximately 20 μM PLE in a cell gives fluorescein levels around 100 μM after a 30 min incubation with 10 μM of compound **6**. Importantly, we observed no apparent alteration in cellular morphology or viability in PLE-expressing cells in these experiments [Fig. S5 *A* and *B* for high magnification confocal and differential interference contrast (DIC) images], perhaps due to sequestration of this esterase in the ER.

To verify that unmasking is specific to PLE-expressing cells, we coexpressed PLE with a red fluorescent protein bearing a nuclear localization sequence (NLS-mCherry) separated by an internal ribosomal entry site (IRES) sequence and incubated these cells with fluorescein-CM_2 (**6**). Fig. 3*A* shows confocal fluorescence microscopy images of a mixture of untransfected HeLa cells (PLE^- cells) and HeLa cells transfected with PLE–IRES–NLS-mCherry (PLE^+ cells), cultured together for 48 h followed by incubation with substrate **6** for 30 min. The green fluorescence from unmasked substrate **6** is correlated with the nuclear red fluorescent signal from mCherry [green-to-red colocalization index = 0.97 ± 0.04 (mean ± SD) (25); Fig. S6 *A*–*C* for additional fields of view] confirming the specificity of this esterase–ester pair.

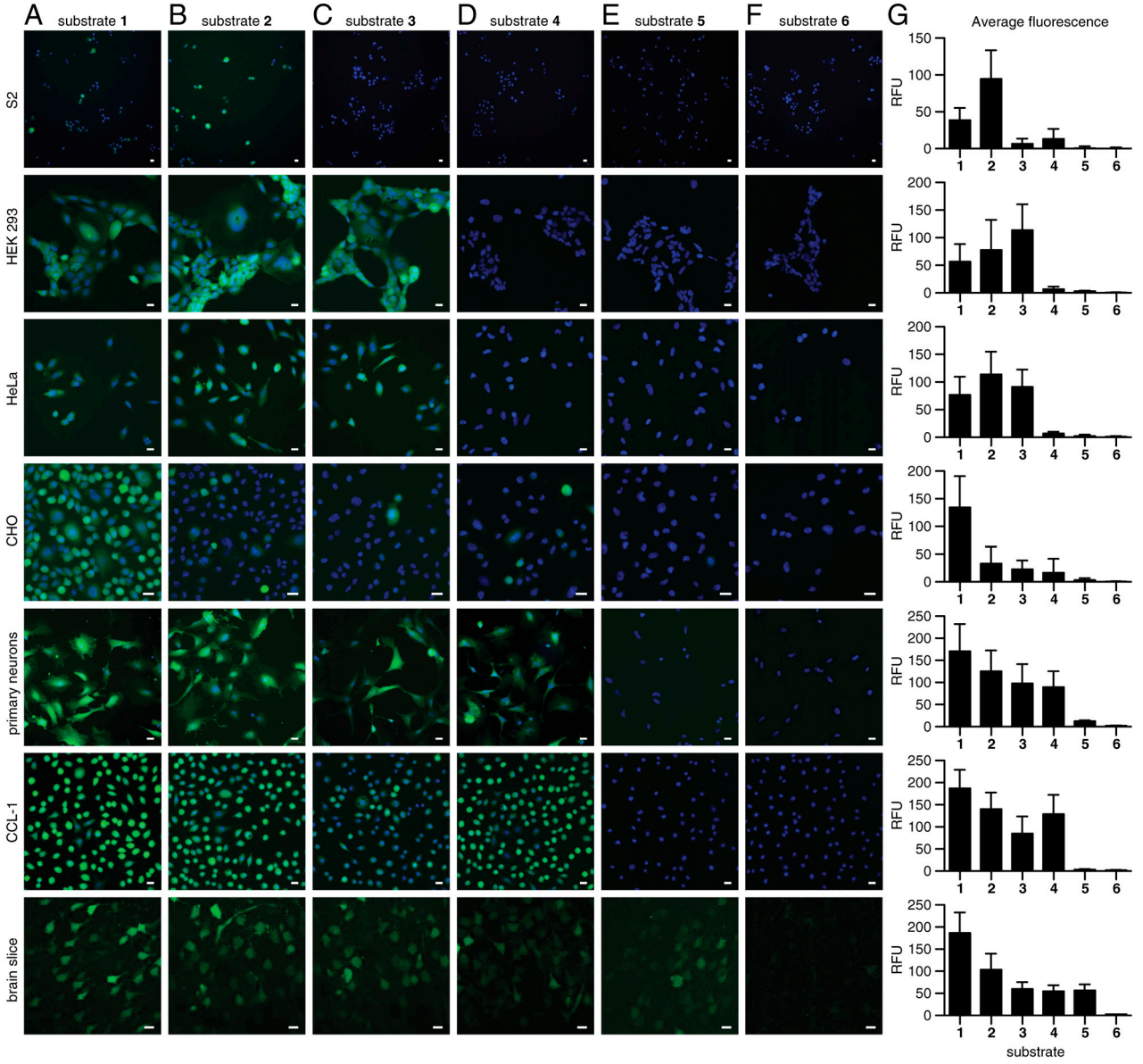

Fig. 2. Fluorescence microscopy and quantitative assessment of hydrolysis of compounds **1**–**6** catalyzed by endogenous cellular esterases. Substrates **1**–**6** (10 μM) were applied to *Drosophila* S2 cells, human embryonic kidney cells (HEK 293), human uterus carcinoma cells (HeLa), Chinese hamster ovary carcinoma cells (CHO), dissociated rat hippocampal primary neuronal culture, mouse fibroblast cells (CCL-1), and mouse cortical brain slice for 1 h and imaged live. (*A*) Substrate **1**. (*B*) Substrate **2**. (*C*) Substrate **3**. (*D*) Substrate **4**. (*E*) Substrate **5**. (*F*) Substrate **6**. Cultured cells were counterstained with Hoechst 33342 and imaged using wide-field fluorescence microscopy. Brain slices were imaged using two-photon microscopy. Magnification was adjusted to ensure several cells were within the imaging field. (Scale bars: 10 μm.) (*G*) Quantification of background-subtracted average cellular fluorescence (relative fluorescence units, RFU) after incubation with substrates **1**–**6**. Error bars show mean ± SD.

We then tested the generality of this system by synthesizing another masked compound based on the red fluorophore 4-carboxyresorufin (17). We applied the acyloxymethyl masking system to both the phenol and carboxylic acid moieties on this dye (Fig. S1*B*). The 4-carboxyresorufin-1-methylcyclopropanecarboxymethyl ether/ester derivative **7** (resorufin-CM_2, Fig. 1*B*) was resistant to hydrolysis by native esterases in HeLa cells and was unmasked only in cells expressing PLE–IRES–GFP as shown in Fig. 3*B* [red-to-green colocalization index = 0.94 ± 0.09 (25); Fig. S6 *D*–*F* for additional fields of view]. This result demonstrates that utility of the α-cyclopropyl ester–PLE system is not confined to the fluorescein structure, but is generalizable, allowing other compounds to be targeted to defined cellular populations.

Esterase-Mediated Unmasking in Cultured Hippocampal Neurons. We then explored the utility and specificity of this system in living neurons. Cultured primary rat hippocampal neurons were transfected with PLE–IRES–NLS-mCherry driven by the human synapsin-1 (*hSYN1*) promoter. Incubation with substrate **6** produced green fluorescence signal exclusively in the PLE^+ neurons (Fig. 4*A*). Time-lapse imaging shows the PLE-catalyzed hydrolysis of substrate **6** reaches saturation within 10 min of application (Fig. S7*B*). The released fluorescein rapidly diffuses throughout the cell; neuronal processes 80 μm from the cell body show half of the maximal cell body intensity within 20 min of application of compound **6** (Fig. S7*C*). In contrast, incubation with the general fluorogenic esterase substrate **1** gives brightly labeled neurons and surrounding astrocytes regardless of PLE expression (Fig. 4*B*), demonstrating the specificity of the PLE–CM pair. As with the previous cell culture experiments we observed no apparent changes in cellular morphology in PLE-expressing neurons (DIC images in Fig. 4 *A* and *B* and Fig. S5 *C* and *D*).

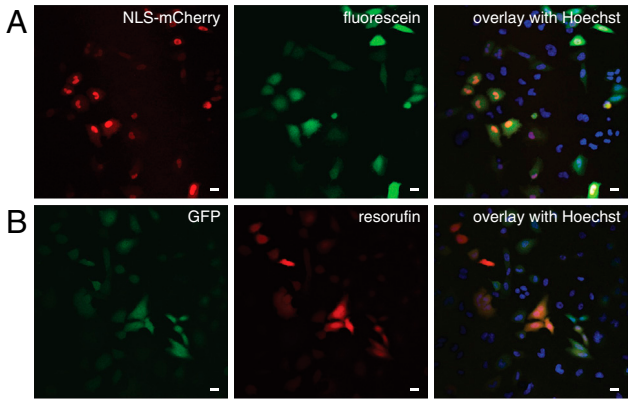

Fig. 3. Cell-specific unmasking of latent fluorophores by PLE in HeLa cells. (*A*) A 1:1 mixture of HeLa cells with or without transfection of PLE–IRES–NLS-mCherry, followed by incubation with substrate **6** (10 μM) and Hoechst 33342 (1 μM) for 30 min. (*B*) A 1:1 mixture of HeLa cells with or without transfection of PLE–IRES–GFP, followed by incubation with substrate **7** (10 μM) and Hoechst 33342 (1 μM) for 30 min. (Scale bars: 10 μm.)

Esterase-Mediated Unmasking in Acute Brain Slice. Given the specificity of this esterase–ester pair in cell culture, we then tested whether we could label specific cell types in a complex biological sample such as brain tissue. We expressed PLE–IRES–mCherry in specific cell types in different brain regions using various transfection techniques. Rat hippocampal astrocytes were transfected using the glial fibrillary acidic protein (*GFAP*) promoter (Fig. 5*A*). The CMV-enhancer, chicken β-actin (*CAG*) promoter, combined with in utero electroporation at E16, gave selective expression in mouse layer 2/3 somatosensory cortical pyramidal neurons (Fig. 5*B*) (26). PLE–IRES–mCherry driven by the *hSYN1* promoter was delivered in layer 2/3 and layer 5 neurons in primary motor cortex (M1) via adeno-associated virus injection at P21. Incubation of brain slices from these animals with substrate **6** showed unmasking of fluorescein (green) that was confined to PLE^+ cells expressing mCherry (red), showing that the esterase–ester system can enable cell-type-specific unmasking of fluorophores in complex tissues. Fig. 5*C* shows green fluorescence signal from the unmasked fluorescein-CM_2 in processes projected from layer 5 neurons. This result shows our method could be useful for labeling small cellular structures (e.g., axons and dendrites) for imaging experiments. Importantly, expression of PLE in neurons did not perturb their electrophysiological properties.

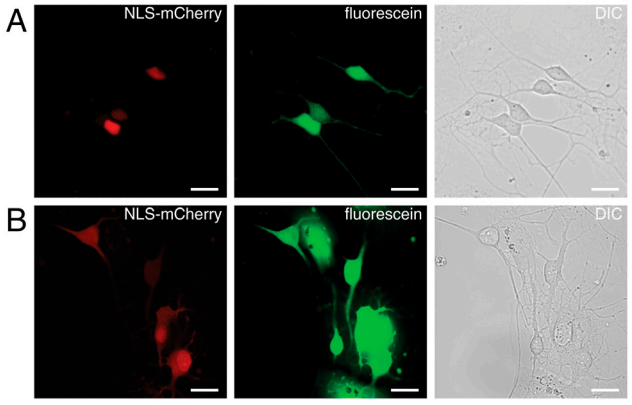

Fig. 4. Cell-type-specific esterase-mediated unmasking in dissociated hippocampal neuron–astrocyte coculture. Neuron–astrocyte coculture was transfected with PLE–IRES–NLS-mCherry driven by the neuron-specific *hSYN1* promoter and incubated with substrate **6** (10 μM) or substrate **1** (10 μM) for 30 min. (*A*) Selective unmasking observed when incubated with substrate **6**. (*B*) Unselective unmasking observed when incubated with substrate **1**. (Scale bars: 10 μm.)

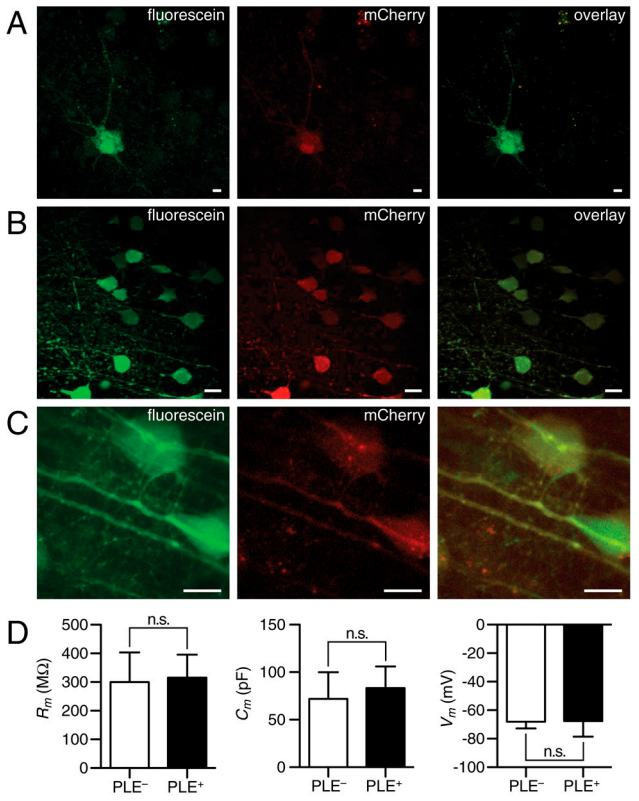

Fig. 5. Cell-type-specific esterase-mediated unmasking in mouse brain slices. (*A*) Two-photon microscopic images of rat hippocampal slice culture transfected with PLE–IRES–mCherry driven by the glial-specific *GFAP* promoter and incubated with compound **6** (10 μM) for 1 h. (*B*) Two-photon microscopic images of cortical layer 2/3 in acute brain slice from mice (P14) in utero electroporated with PLE–IRES–mCherry under the *CAG* promoter at E16, and incubated with compound **6** (10 μM) for 1 h. (*C*) Two-photon microscopic images of cortical layer 2/3 in acute brain slice from mice (P35) transduced with adeno-associated viral vector for PLE–IRES–mCherry under the *hSYN1* promoter, and incubated with compound **6** (10 μM) for 1 h. (Scale bars: 10 μm.) (*D*) Comparison of input resistance (R_m), cell capacitance (C_m), and resting membrane potential (V_m) of PLE^- and PLE^+ neurons in acute brain slice. Error bars show mean ± SD, n.s. is not significant, $p > 0.05$.

PLE^+ cells exhibited similar resting membrane potential, input resistance, and capacitance compared to PLE^- neurons (Fig. 5*D*), demonstrating that active PLE can be expressed in sensitive neural tissue without compromising cellular properties.

Illuminating Gap Junctions. In addition to labeling individual cells, we determined whether PLE-mediated unmasking of fluorescein could map cellular networks interconnected by gap junctions. Gap junction intercellular communication is a critical biological process, modulating neural connectivity, cardiac cell activity, pancreatic β-cell function, and cancer cell biogenesis (27–29). The classic method of visualizing gap junction connectivity and function involves charging specific cells with a small (<1 kD) molecule such as a fluorophore or biotin derivative that is permeable to gap junctions of various compositions (30). Current techniques to introduce small molecules into cells are invasive (31, 32), inefficient (6, 33), or limited in the number of cells that can be studied at one time (34). We reasoned the PLE–CM enzyme–substrate system could provide an alternative method to these techniques by enabling noninvasive introduction of a dye in specific cells and real-time visualization of gap junction connectivity in a cellular network.

To investigate the utility of the PLE–CM system in mapping gap junction connectivity, we used WB-F344 rat liver epithelial cells, which express high levels of endogenous connexins, a key

component of mammalian gap junctions (Fig. S8 *A–F*) (28). Cultured cells were first transfected with PLE–IRES–NLS-mCherry and then mixed with excess untransfected cells to achieve a sparse distribution of PLE^+ cells within a larger population of PLE^- cells. After incubation of this mixed population of cells with α-cyclopropyl substrate **6**, we observed fluorescein signal in both PLE^+ and adjoining PLE^- cells with the fluorescence intensity decreasing with distance from PLE^+ cells (Fig. 6*A*). When cells were treated with 12-*O*-tetradecanoylphorbol-13-acetate (TPA), which activates protein kinase C, thereby inhibiting gap junction intercellular communication (35), the green fluorescence was retained solely in PLE^+ cells (Fig. 6*B*). As with the other cell types, the expression of PLE did not cause apparent cytotoxicity in this cell line (Fig. S5 *E–G*). We next investigated dynamics of gap junction connectivity between PLE^+ cells and PLE^- cells using fluorescence recovery after photobleaching (FRAP) (28). The dynamic imaging data show that the fluorescein unmasked in PLE^+ cells is able to quickly diffuse to PLE^- cells through gap junctions with a rate of fluorescence recovery of approximately 20% per minute (Fig. S8*G*, Movie S2), consistent with other gap junction FRAP experiments (28). Therefore, the rapid and cell-specific unmasking of fluorescein enables facile static and dynamic imaging assays of gap junction connectivity in live systems.

Cell-Specific Pharmacology. We then tested the utility of this strategy to deliver a pharmacological agent in a cell-specific manner. Monastrol (**8**, Fig. 7*A*) is a reversible small molecule inhibitor of the kinesin Eg5 mitotic motor. Eg5 is responsible for polarization of microtubules during cell division; inhibition by compound **8** blocks mitosis and gives a distinct monopolar spindle phenotype (36). Structure–activity relationship studies have demonstrated that substitution on the phenolic oxygen of monastrol abolishes this biological activity (37), implying that attachment of the CM motif at this position could allow pharmacological control of mitosis in a genetically defined manner. As shown in Fig. 7*A*, alkylation of compound **8** with halomethyl ester **9** gave monastrol-CM (**10**). Incubation of compound **10** with PLE in vitro showed clean conversion of the molecule to monastrol (**8**) without detectable cleavage of the ethyl ester group (Fig. S9*A*).

To test the cellular specificity of the PLE–monastrol-CM system, we added monastrol (**8**; 50 μM), monastrol-CM (**10**; 50 μM), or a DMSO control to transfected (PLE^+) or untransfected (PLE^-) HeLa cells upon release from a double thymidine block (36). After incubation with the pharmacological agent, cells were fixed, stained for chromatin and microtubules, and the percentage of cells in M phase showing apparent altered mitotic spindles was quantified as shown in Fig. 7*B*. Representative fluorescence microscopy images are shown in Fig. S9 *B* and *C*. As expected, PLE^- HeLa cells in M phase that are treated with monastrol (**8**) exhibit an increased frequency of altered mitotic spindles. This phenotype is observed in approximately 30% of mitotic cells and is independent of PLE expression. Alkylation of monastrol blocks its biological activity; incubation of monastrol-CM (**10**) with PLE^- cells shows no significant occurrence of altered mitotic spindles above the DMSO control. Treatment of PLE^+ cells with monastrol-CM, however, gives the monopolar spindle phenotype with approximately 60% occurrence. The incidence of the distorted spindle phenotype observed between PLE^+ and PLE^- cells when treated with monastrol-CM (**10**) is significantly different (unpaired Student's *t* test, $p = 0.0007$), thus demonstrating this esterase–ester system is able to target pharmacological agents with cellular specificity. The higher efficacy of compound **10** compared to parent compound **8** in PLE^+ cells is likely due to the increased cellular permeability resulting from the masking of the polar phenol with the lipophilic CM group.

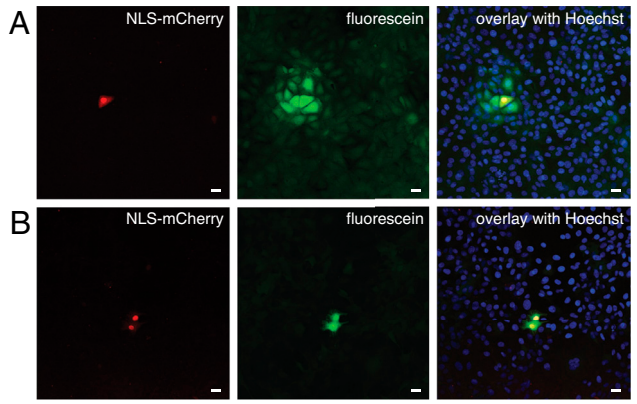

Fig. 6. Noninvasive imaging of gap junction permeability in living cells using an esterase–ester system. WB-F344 cells were first transfected with PLE–IRES–NLS-mCherry for 24 h. Transfected cells were mixed with untransfected cells and incubated at 37 °C for an additional 24 h. (*A*) Cells incubated with substrate **6** (10 μM) and Hoechst 33342 (1 μM) for 30 min. (*B*) Cells pretreated with 12-*O*-tetradecanoylphorbol-13-acetate (TPA, 100 nM) for 30 min prior to addition of compound **6** (10 μM) and Hoechst 33342 (1 μM). (Scale bars: 10 μm.)

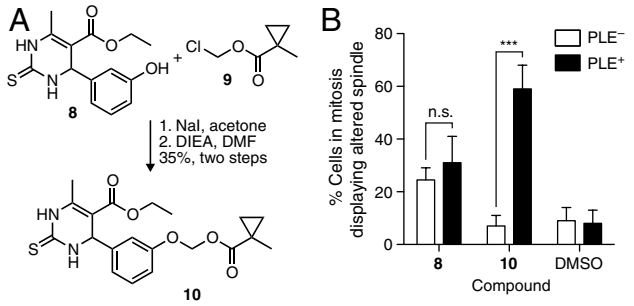

Fig. 7. Cell-specific pharmacology. (*A*) Synthesis of monastrol-CM (**10**). (*B*) Prevalence of an altered spindle phenotype in PLE^- cells and cells transfected with PLE–IRES–mCherry (PLE^+ cells) when released from the double thymidine block to 50 μM monastrol (**8**), 50 μM monastrol-CM (**10**), or DMSO control (0.1% vol/vol) as a percentage of all mitotic cells. Error bars show mean ± SD, n.s. is not significant, $p > 0.05$, *** $p < 0.001$.

Conclusion

We developed a generalizable cell-specific delivery strategy to augment the molecular specificity of small molecules. Rather than search for a selective enzyme–substrate pair in distal species, we investigated the esterases, which have long been exploited for general cellular delivery of small organic molecules. We synthesized a unique family of stable fluorogenic esterase substrates and systematically incubated them with a number of cell types and tissues, assessing the specificity of native esterases in different cell types at the whole-cell level. Esterases from different species were found to exhibit divergent activity toward synthetic substrates in a cellular context. We exploited these differences and identified a selective esterase–ester pair capable of the targeted delivery of small molecules in complex environments with cellular specificity. The described α-cyclopropyl ester moiety has low molecular mass, is synthetically accessible, and is easily incorporated into existing strategies to mask polar functionalities using ester groups, such as the widely used, but cell-type-unselective, acetoxymethyl ether/ester system (10, 11). The complementary exogenous enzyme, PLE, efficiently catalyzes the hydrolysis of this ester bond and does not show obvious effects on cellular properties, even in highly sensitive neuronal tissue. The compatibility of this promiscuous esterase with normal cellular function is likely due to, at least in part, the natural localization of PLE in the ER (7, 20). Both the rapid evaluation of enzyme–substrate pairs using a series of fluorogenic compounds and sequestration of active enzymes in subcellular compartments may be useful strategies to apply to other enzyme-based targeting systems.

This PLE–CM esterase–ester pair shows broad utility in labeling and perturbing cell populations of a particular type. Rapid, cell-specific introduction of small fluorescent molecules was used to label defined populations in culture and particular cell types in neural tissue. Introduction of fluorescent dyes into living cells using the esterase–ester combination allowed facile mapping of gap junction connectivity between cell populations and could provide a platform for high content screening of agents that modulate gap junction connectivity. Finally, targeted delivery of a pharmacological agent allowed control of the cell cycle with cellular specificity. This general approach can be extended to other small organic compounds bearing appropriate maskable functionality to control disparate cellular behaviors such as neural activity, gene transcription, and protein synthesis with genetic specificity and high spatiotemporal precision (38).

This systematic study of esterase specificity on a whole-cell level increases the potential of esterases as tools for biological research. The diversity of esterases across biological systems makes this protein class a potentially rich—and largely untapped—resource for developing selective enzyme–substrate pairs. Expansion of the ester-fluorophore substrate library and further assessment of endogenous and exogenous esterase activity will provide additional esterase–ester systems for small molecule delivery in cells, tissues, or whole animals. Finally, we note the interesting patterns of cell line-selective fluorophore unmasking (Fig. 2). Evaluation of other cells and tissues may reveal additional differences in endogenous cellular esterase activity between disparate cell types and species. These distinctions in endogenous esterase activity might also be exploited for the delivery of small molecules and for identifying esterase biomarkers to facilitate molecular diagnosis of disease states (39).

Materials and Methods

Cell Culture, Gene Transfection, and Imaging. Cell lines were obtained from American Type Culture Collection (ATCC) and cultivated according to instructions. Primary hippocampal neurons were obtained from P0 rat pups cultured by dissection, papain-based dissociation, and plating onto glass-bottom MatTek plates and then cultured in DMEM/B27 media. Transfection was performed using a jetPEI DNA Transfection Kit or an Amaxa Nucleofector Kit. Cellular fluorescence was imaged using an Olympus IX81 wide-field fluorescence microscope, a Nikon Eclipse TI fluorescence microscope, or a Zeiss LSM 510 fluorescence microscope.

Brain Slice Preparation and Imaging. Hippocampal slice cultures were prepared using standard methods and transfection was performed by biolistic gene transfer. Acute brain slices were prepared from mice at P14–35. Transfection was performed by in utero electroporation at E16 or by viral injection into the primary motor cortex (M1) of mice at P21. Fluorescence images of hippocampal slice cultures and acute slices were acquired using a custom-built, two-photon laser-scanning microscope equipped with a Ti:Sapphire laser and a 60×, 0.9 N.A. objective (Olympus).

For further information on synthetic methods, cell culture, transfection, imaging, and other protocols, *SI Materials and Methods*.

ACKNOWLEDGMENTS. We are grateful to H.R. White and S.G. Winfrey for cell culture assistance, J.S. Marvin for protein purification, B.M. Hooks for brain slice assistance, and R.J. Johnson, R.T. Raines, and K. Svoboda for contributive discussions. The Howard Hughes Medical Institute supported this work.

1. Jiang T, Xing B, Rao J (2008) Recent developments of biological reporter technology for detecting gene expression. *Biotechnol Genet Eng Rev* 25:41–76.
2. Nirenberg S, Cepko C (1993) Targeted ablation of diverse cell classes in the nervous system in vivo. *J Neurosci* 13:3238–3251.
3. Gao W, Xing B, Tsien RY, Rao J (2003) Novel fluorogenic substrates for imaging β-lactamase gene expression. *J Am Chem Soc* 125:11146–11147.
4. Ng DN, Fromherz P (2011) Genetic targeting of a voltage-sensitive dye by enzymatic activation of phosphonooxymethyl-ammonium derivative. *ACS Chem Biol* 6:444–451.
5. Weiss DJ, Liggitt D, Clark JG (1999) Histochemical discrimination of endogenous mammalian-galactosidase activity from that resulting from *lac-Z* gene expression. *Histochem J* 31:231–236.
6. Subauste MC, et al. (2001) A catalytic antibody produces fluorescent tracers of gap junction communication in living cells. *J Biol Chem* 276:49164–49168.
7. Potter PM, Wolverton JS, Morton CL, Wierdl M, Danks MK (1998) Cellular localization domains of a rabbit and a human carboxylesterase: Influence on irinotecan (CPT-11) metabolism by the rabbit enzyme. *Cancer Res* 58:3627–3632.
8. Vass SO, Jarrom D, Wilson WR, Hyde EI, Searle PF (2009) *E. coli* NfsA: An alternative nitroreductase for prodrug activation gene therapy in combination with CB1954. *Br J Cancer* 100:1903–1911.
9. Curado S, Stainier D, Anderson R (2008) Nitroreductase-mediated cell/tissue ablation in zebrafish: A spatially and temporally controlled ablation method with applications in developmental and regeneration studies. *Nat Protoc* 3:948–954.
10. Testa B, Mayer JM (2003) *Hydrolysis in Drug and Prodrug Metabolism: Chemistry, Biochemistry, and Enzymology* (Verlag Helvetica Chimica Acta, Zürich, Switzerland), pp 365–534.
11. Lavis LD (2008) Ester bonds in prodrugs. *ACS Chem Biol* 3:203–206.
12. Rehberg M, Lepier A, Solchenberger B, Osten P, Blum R (2008) A new non-disruptive strategy to target calcium indicator dyes to the endoplasmic reticulum. *Cell Calcium* 44:386–399.
13. Satoh T, Hosokawa M (2006) Structure, function and regulation of carboxylesterases. *Chem-Biol Interact* 162:195–211.
14. Brüsehaber E, Böttcher D, Bornscheuer UT (2009) Insights into the physiological role of pig liver esterase: Isoenzymes show differences in the demethylation of prenylated proteins. *Bioorg Med Chem* 17:7878–7883.
15. Bender DM, et al. (2008) Cyclopropanecarboxylic acid esters as potential prodrugs with enhanced hydrolytic stability. *Org Lett* 10:509–511.
16. Yamazaki Y, Kageyama Y, Okuno H (1995) Direct evaluation of stereoselectivity of cancer esterases by polyacrylamide gel electrophoresis coupled with activity staining with chiral naphthyl esters. *Anal Biochem* 231:295–300.
17. Lavis LD, Chao TY, Raines RT (2011) Synthesis and utility of fluorogenic acetoxymethyl ethers. *Chem Sci* 2:521–530.
18. Stok JE, et al. (2004) Identification, expression, and purification of a pyrethroidhydrolyzing carboxylesterase from mouse liver microsomes. *J Biol Chem* 279:29863–29869.
19. Lange S, Musidlowska A, Schmidt-Dannert C, Schmitt J, Bornscheuer U (2001) Cloning, functional expression, and characterization of recombinant pig liver esterase. *ChemBioChem* 2:576–582.
20. Medda S, Proia RL (1992) The carboxylesterase family exhibits C-terminal sequence diversity reflecting the presence or absence of endoplasmic-reticulum-retention sequences. *Eur J Biochem* 206:801–806.
21. Markwardt ML, et al. (2011) An improved cerulean fluorescent protein with enhanced brightness and reduced reversible photoswitching. *PloS One* 6:e17896.
22. Le Gall S, Neuhof A, Rapoport T (2004) The endoplasmic reticulum membrane is permeable to small molecules. *Mol Biol Cell* 15:447–455.
23. Lizak B, et al. (2006) Translocon pores in the endoplasmic reticulum are permeable to small anions. *Am J Physiol Cell Physiol* 291:C511–C517.
24. Hsu CF, Dervan PB (2008) Quantitating the concentration of Py-Im polyamide-fluorescein conjugates in live cells. *Bioorg Med Chem Lett* 18:5851–5855.
25. Jaskolski F, Mulle C, Manzoni OJ (2005) An automated method to quantify and visualize colocalized fluorescent signals. *J Neurosci Methods* 146:42–49.
26. Saito T, Nakatsuji N (2001) Efficient gene transfer into the embryonic mouse brain using in vivo electroporation. *Dev Biol* 240:237–246.
27. Goodenough DA, Goliger JA, Paul DL (1996) Connexins, connexons, and intercellular communication. *Annu Rev Biochem* 65:475–502.
28. Trosko JE, Ruch RJ (1998) Cell-cell communication in carcinogenesis. *Front Biosci* 3:d208–d236.
29. Bennett MVL, Zukin RS (2004) Electrical coupling and neuronal synchronization in the mammalian brain. *Neuron* 41:495–511.
30. Abbaci M, Barberi-Heyob M, Blondel W, Guillemin F, Didelon J (2008) Advantages and limitations of commonly used methods to assay the molecular permeability of gap junctional intercellular communication. *BioTechniques* 45:33–62.
31. El-Fouly MH, Trosko JE, Chang CC (1987) Scrape-loading and dye transfer: A rapid and simple technique to study gap junctional intercellular communication. *Exp Cell Res* 168:422–430.
32. Meda P (2000) Probing the function of connexin channels in primary tissues. *Methods* 20:232–244.
33. Goldberg GS, Bechberger JF, Naus CC (1995) A pre-loading method of evaluating gap junctional communication by fluorescent dye transfer. *BioTechniques* 18:490–497.
34. Guo YM, et al. (2008) Imaging dynamic cell-cell junctional coupling in vivo using Trojan-LAMP. *Nat Methods* 5:835–841.
35. Ren P, Mehta PP, Ruch RJ (1998) Inhibition of gap junctional intercellular communication by tumor promoters in connexin43 and connexin32-expressing liver cells: Cell specificity and role of protein kinase C. *Carcinogenesis* 19:169–175.
36. Kapoor TM, Mayer TU, Coughlin ML, Mitchison TJ (2000) Probing spindle assembly mechanisms with monastrol, a small molecule inhibitor of the mitotic kinesin, Eg5. *J Cell Biol* 150:975–988.
37. Maliga Z, Mitchison TJ (2006) Small-molecule and mutational analysis of allosteric Eg5 inhibition by monastrol. *BMC Chem Biol* 6, 10.1186/1472-6769-6-2.
38. Koya E, et al. (2009) Targeted disruption of cocaine-activated nucleus accumbens neurons prevents context-specific sensitization. *Nat Neurosci* 12:1069–1073.
39. Afrimzon E, et al. (2008) Intracellular esterase activity in living cells may distinguish between metastatic and tumor-free lymph nodes. *Clin Exp Metastasis* 25:213–224.